Materials & Design 267 (2026) 116226

Contents lists available at ScienceDirect

Materials & Design

journal homepage: www.elsevier.com/locate/matdes

Growth twins within (Al_3(Sc,Ti) + α-Al) eutectic cells enable novel grain refinement in recycled Al alloys

Zhongping Que *, Zhichao Niu, Chamini L. Mendis, Raluca Florentina Negrea, Zhongyun Fan

Brunel Centre for Advanced Solidification Technology (BCAST), Brunel University London, Uxbridge, Middlesex UB8 3PH, UK

ARTICLE INFO

Keywords:
α-Al Growth Twins
(Al+Al_3(Sc,Ti)) eutectic cells
Grain refinement
Spatial confinement
Multicomponent recycled Al alloys

ABSTRACT

Designing sustainable aluminium alloys with superior mechanical performance requires effective microstructural control during solidification. In this study, a cross-over recycled wrought aluminium alloy system spanning the 1xxx–7xxx series was designed with maximum impurity tolerance. A grain refinement strategy using hypo-eutectic Sc additions was developed to simultaneously refine grains and second-phase particles. A previously unreported grain refinement mechanism was identified in this multicomponent recycled alloy, where the growth of α-Al grains is constrained by a network of (Al + Al_3(Sc,Ti)) eutectic cells rather than by classical heterogeneous nucleation. Remarkably, α-Al growth twins were observed within these eutectic cells, a crystallographic feature rarely reported in high stacking-fault-energy aluminium. Atomic-scale characterization using scanning transmission electron microscopy (STEM) reveals the structural characteristics associated with this phenomenon. These findings provide a new pathway for microstructural control in complex recycled aluminium alloys and offer design principles for next-generation sustainable lightweight materials with enhanced mechanical performance.

1. Introduction

Aluminium recycling plays a critical role in reducing carbon emissions, conserving natural resources, and securing global supply chains [1,2]. However, the increasing compositional complexity of recycled aluminium alloys presents significant challenges for microstructure control during solidification [3,4]. Impurity accumulation and multi-element interactions often reduce the effectiveness of conventional grain-refinement strategies, making the development of resilient alloy systems capable of maintaining microstructural stability under repeated recycling increasingly important.

Grain refinement is widely used to improve casting quality and mechanical performance in aluminium alloys by reducing defects such as hot tearing and refining the solidification structure [5,6]. Conventional grain refinement strategies primarily rely on heterogeneous nucleation facilitated by TiB_2-based master alloys and solute-induced growth restriction [7–10]. While effective in many commercial alloys, their performance can be significantly affected by solute interactions and impurity accumulation in recycled materials, which may alter nucleation behaviour and reduce grain refinement efficiency [11].

Among alloying elements, Scandium (Sc) is known to be one of the most potent modifiers of aluminium microstructures [12–14]. Sc additions can form the coherent $L1_2$-structured Al_3Sc phase, which contributes to significant strengthening and thermal stability in aluminium alloys. In hypoeutectic compositions, Sc can also participate in eutectic reactions, forming (Al + Al_3Sc) microstructures that influence solidification behaviour and grain structure development.

Another long-standing assumption in aluminium metallurgy concerns the formation of twins in α-Al [15–22]. The twinning ability of FCC metals has been extensively investigated, typically through first-principles density functional theory (DFT) calculation [16]. The inherent difficulty in forming twins in FCC metals such as Al is well understood, primarily due to the availability of sufficient and high stacking fault energy (SFE) ~120–165 mJ/m^2 [17]. Prior theoretical studies have suggested that alloying Al with scandium can significantly reduce its SFE, especially at concentrations above 0.5 wt.%, potentially enabling twin formation [18,19]. However, no experimental validation of this prediction during casting had been reported although a few cases of Al twins were reported through deformation [20–22]. In this work, we present the first experimental evidence of twin formation in Al during

* Corresponding author.
E-mail address: Zhongping.Que@brunel.ac.uk (Z. Que).

https://doi.org/10.1016/j.matdes.2026.116226
Received 14 March 2026; Received in revised form 2 May 2026; Accepted 13 May 2026
Available online 14 May 2026

solidification process under the equivalent condition to industrial DC casting (at 3.5 K/s), and we demonstrate a nucleation-induced mechanism responsible for this phenomenon.

In this work, a previously unrecognized grain-refinement mechanism in a recycled multi-component aluminium alloy induced by hypoeutectic Sc addition will be reported. Instead of promoting grain refinement through primary heterogeneous nucleation, refinement occurs via Spatial confinement of α-Al grains by a network of (Al + Al_3(Sc, Ti)) eutectic cells. Remarkably, α-Al twins are observed within these cells, revealing a previously unreported crystallographic feature in aluminium alloys. These findings provide new insight into grain refinement mechanisms in complex recycled systems and suggest alternative pathways for microstructure control in sustainable aluminium alloys.

2. Experimental

The studied alloy has the nominal composition Al-1.33Si-1.28Mg-0.97Cu-0.88Zn-0.51Fe-0.57Mn-0.14Cr-0.09Ti, which was based on the average compositions of selected wrought alloys from the A1050, A2024, A3003, A4043, A5052, A6082, and A7075 series, using the upper limit of each alloying element [23]. This simulated recycled alloy (RA) was produced from commercial-purity (CP) Al (99.9 wt.%), CP Mg (>99.95 wt.%), CP Zn (>99.95 wt.%), and various master alloys including Al-50 wt.% Si, Al-20 wt.% Mn, Al-10 wt.% Ti, Al-20 wt.% Cr, and Al-38 wt.% Fe. To compensate for the vaporization of volatile elements such as Mg during melting, an additional 3 wt.% CP-Mg was added, ensuring that the final chemical composition closely matched the nominal targets. Sc additions of 0.1, 0.3 and 0.5 wt.% were introduced via an Al-2Sc master alloy, with 0.2 wt.% Al-5Ti-1B used for comparison.

CP-Al and all master alloys were first melted at 800 ℃ in an electric resistance furnace with thorough stirring to ensure complete dissolution. CP-Mg and CP-Zn, wrapped in Al foil and preheated to 200 ℃, were then added to the melt. After full dissolution, the melt was held for 30 min before slag removal. The alloys were cast into a Tp-1 mould [24] which was preheated to 380 ℃, provides a cooling rate of 3.5 K/s at 38 mm from the bottom, simulating industrial direct chill (DC) casting conditions. Alloys were poured at 750 ℃.

Metallographic specimens were prepared using standard procedures. As-cast microstructures were examined with a Zeiss optical microscope and AxioVision 4.3 software. SEM and EBSD analyses were performed on a Zeiss Crossbeam 340 FIB-SEM at 20 kV, with EBSD step sizes of 5 μm for low-magnification and 0.5 μm for high-magnification scans. TEM samples were prepared via FIB milling on the same instrument and observed using a Cs-corrected SPECTRA 300 TEM (Thermo Fisher Scientific) equipped with a Super-X EDS detector at 200 kV.

A significant difference in the observed grain refinement was identified when comparing polarized optical microscopy (OM) and EBSD IPF mapping, which arises from their fundamentally different contrast mechanisms. Polarized optical microscopy and EBSD maps are based on fundamentally different mechanisms. Polarized OM generates contrast from optical anisotropy (birefringence) and/or interference effects in surface of the sample investigated. Thus, information that may be received from polarised microscopy is limited to 2D information and any misorientation associated in the 3rd dimension is not captured and only misorientations in the 2D plane may be observed. EBSD data sets contained Kikuchi maps that provide data in 3D rather than the 2D thus more misorientation information can be acquire from the EBSD maps. Polarized OM was employed to characterize the size and morphology of α-Al dendrites. In contrast, EBSD IPF mapping was utilized to investigate local crystallographic orientation and misorientation variations induced by the addition of Sc.

3. Results

3.1. Grain refinement by Sc compared to a commercial Al-Ti-B grain refiner

Fig. 1 shows the microstructure of the studied recycled alloy (Al-1.33Si-1.28Mg-0.97Cu-0.88Zn-0.51Fe-0.57Mn-0.14Cr-0.09Ti) without and with additions of 0.2 wt.% Al-5Ti-1B or 0.3–0.5 wt.% Sc. Set-1 (EBSD-IPF images) highlights several key points: the grain refinement achieved by hypoeutectic Sc addition is markedly more effective than that of the commercial Al-5Ti-1B refiner, but the underlying refinement mechanisms are fundamentally different. Quantified grain sizes, secondary dendrite arm spacing, and grain refinement efficiencies according to anodized optical and EBSD are listed in Table 1, respectively.

With 0.2 wt.% Al-5Ti-1B, the average α-Al grain size decreased from 504 ± 24 μm to 263 ± 11 μm, corresponding to a grain refinement efficiency of 47.8 %. In this case, secondary phase particles (SPPs) were pushed toward grain boundaries and became coarser compared with the as-cast RA alloy. In the reference RA (Fig. 1a-2), SPPs were relatively evenly distributed along the secondary dendrite arms and grain boundaries. After Al-5Ti-1B addition (Fig. 1b-2), SPPs concentrated at grain boundaries due to thickened dendritic arms and a reduction in intra-granular SPPs. The difference in quantification between optical anodized samples and EBSD results for these two samples is relatively small compared with those containing Sc additions.

EBSD and anodizing provide complementary insights into grain refinement in Al alloys with Sc additions. EBSD-IPF maps clearly resolve α-Al grains and grain boundaries over large areas, enabling precise grain size measurements. In contrast, anodized samples highlight dendritic and inter-dendritic morphologies and reveal the distribution of secondary phase particles (SPPs). Figs. 1c–e show the effect of Sc addition: for RA + 0.3 wt.% Sc, EBSD, SEM-BSD, and anodized optical images reveal a distinctly different refinement behaviour. Numerous “small grains” appear within the larger α-Al grains, exhibiting twin-like crystallographic features in EBSD-IPF maps (Fig. 1d-1). These features are less visible in SEM-BSD images (Fig. 1c-2) and in anodized optical image (Fig. 1c-3) but become apparent at higher magnification (Fig. 1d-2, and d-3). Detailed analysis confirms that these “small grains” are in fact eutectic cells containing fine SPPs with boundary segregation. Surrounding Chinese-script Fe-containing intermetallic compounds (IMCs) form at the grain boundary ends of these cells, restricting α-Al grain growth. Anodized images further show that these eutectic cells are distributed along secondary dendrite arms and at grain boundaries (Figs. 1c-3, d-3).

The unique refinement mechanism of Sc requires quantification by both EBSD and anodizing. Anodized samples indicate a 28.6 % reduction in primary α-Al grain size, while EBSD-IPF maps show an 82.4 % refinement when accounting for both α-Al grains and eutectic cells. The combined effect of α-Al grain subdivision and eutectic cells (“divorcing effect”) represents the true grain refinement.

At 0.5 wt.% Sc, maximum α-Al grain refinement is achieved before the formation of primary Al_3Sc particles, which can otherwise reduce the refinement effect (will be published in the other paper). RA + 0.3 wt.% Sc yields ~28.6 % α-Al grain refinement, while 0.5 wt.% Sc achieves 48.0 % if quantified from anodized sample with optical technique, comparable to the Al-5Ti-1B case. When considering the contribution of eutectic cells and twinning, EBSD indicates an overall grain refinement of 84.9 % with addition of 0.5wt.% Sc, substantially higher than the 82.4 % observed for 0.3 wt.% Sc.

In RA + 0.5 wt.% Sc, the microstructure is uniformly refined (Fig. 1e-1). Eutectic cells enlarge, primary α-Al grains become less distinct, and SEM-BSD images (Fig. 1e-2) show well-distributed SPPs without coarsening or boundary segregation. Twinned eutectic cells are more pronounced in anodized samples (Fig. 1e-3), with increased size and number density compared to RA + 0.3 wt.% Sc. Microstructural examination using polarised light microscopy did not illustrate the differences

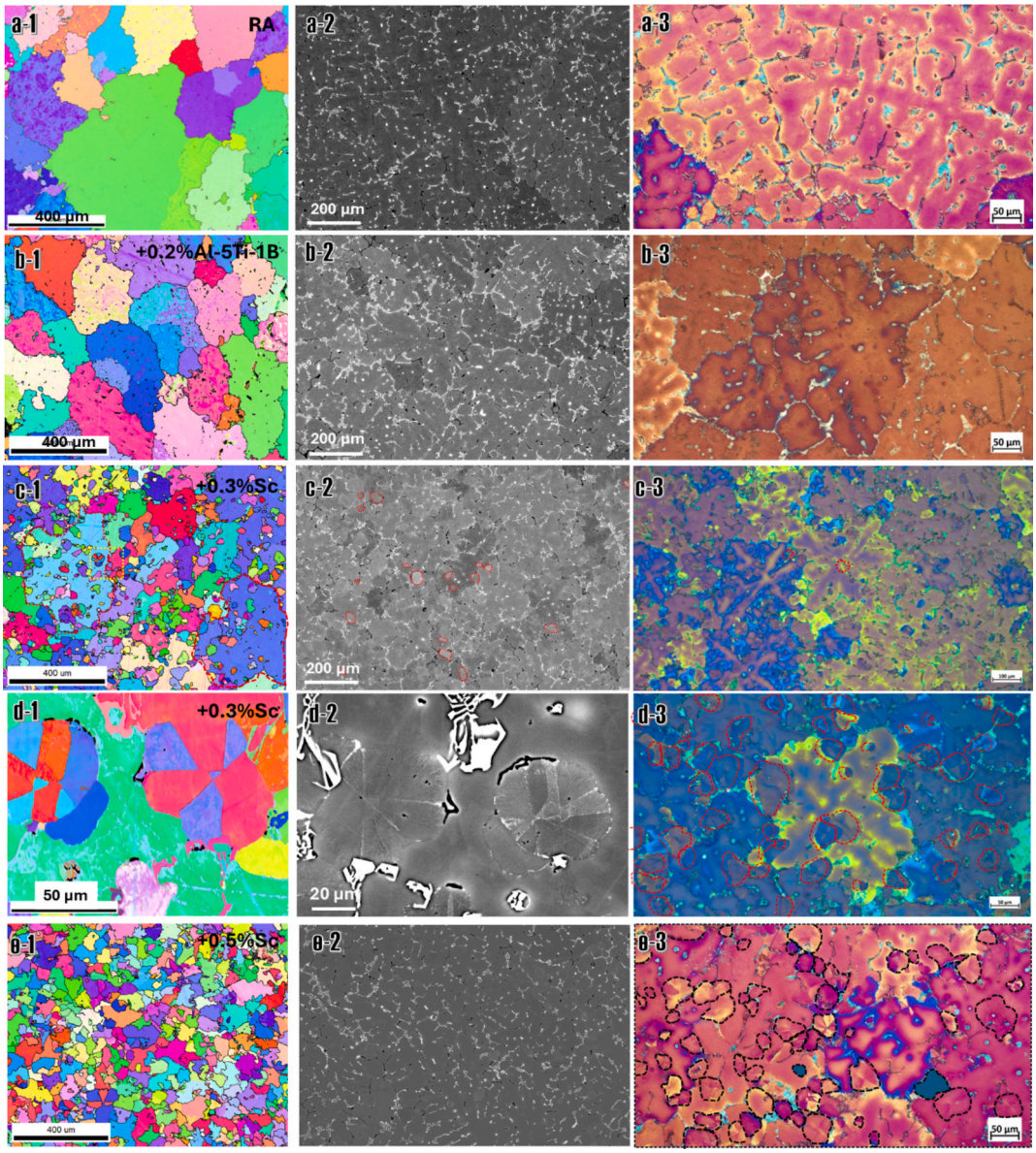

Fig. 1. Microstructures of the studied recycled alloy (Al-1.33Si-1.28Mg-0.97Cu-0.88Zn-0.51Fe-0.57Mn-0.14Cr-0.09Ti) cast at 3.5 K/s from 750 ℃. Set-1: EBSD-IPF images; Set-2: SEM-BSD images; Set-3: anodized optical images. (a) Reference RA without grain refiner or Sc; (b) RA + 0.2 wt.% Al-5Ti-1B; (c) RA + 0.3 wt.% Sc; (d) higher magnification of RA + 0.3 wt.% Sc; (e) RA + 0.5 wt.% Sc.

in orientation within the same dendrite while EBSD investigations illustrate this clearly. In Fig. 2, variation in orientation between dendritic arms within a dendrite is illustrated and the orientation of Al crystals of each dendrite is illustrated within the micrograph. Even though there is a misorientations of 53-60^{o} between many of the dendrites the plane parallel to the surface of the dendrite observed is a low symmetry indexed plane close to 001 planes. As such even through there is a large crystallographic misorientation between each of the dendritic arms this cannot be deciphered through optical microscopy techniques.

3.2. *Twinned eutectic cells of (Al_3(Sc,Ti) + α-Al)*

The eutectic cells observed in RA + 0.3 wt.% Sc were further investigated using STEM, where α-Al growth twins were first identified within these cells. Fig. 3a shows a low-magnification bright-field TEM image highlighting a twin boundary (TB), while the corresponding selected area electron diffraction (SAED) patterns in Figs. 3d and 3e confirm the presence of twinning in α-Al with {112} twin planes. Figs. 3b and 3c present HAADF-STEM images illustrating the atomic arrangement at the twin boundary, including stacking faults and solute segregation associated with the boundary. Fig. 3f shows the FFT pattern corresponding to Fig. 3c, clearly demonstrating the {112} twinning plane. Figs. 3g-i presents HAADF image and corresponding STEM-EDS mapping at the twin boundary, revealing the segregation of Cu atoms along the twin boundary.

Fig. 3j shows the STEM–EDS spectrum acquired at the TB from the region highlighted by the yellow frame in Fig. 3g. The corresponding quantified composition is presented in the table in Fig. 3k. The results indicate an increased Cu concentration at the twin boundary, corresponding to the TB segregation (Fig. 3i), accompanied by relatively lower concentrations of the other elements. Further STEM-EDS line scans along the TB are shown in Fig. 3l and Fig. 3m, which reveal reduced concentrations of Sc and Ti at the TB.

The interface between the eutectic cells and the Al matrix was also examined with STEM and shown in Fig .4. The STEM-EDS mapping demonstrates that the fine precipitates/SPPs within the eutectic are Sc-

Table 1
Grain size, second dendritic arm spacing and refinement of RA without and with additions of grain refiner and Sc.

Optical Anodized	RA	RA + 0.2Al5Ti1B	RA + 0.1Sc	RA + 0.3Sc	RA + 0.5Sc
Grain size (μm)	504 ± 24	263 ± 11	498 ± 9	360 ± 7	262 ± 7
Grain refinement	-	47.8 %	1.2 %	28.6 %	48.0 %
SDAS (μm)	30.6 ± 0.7	32.1 ± 2.7	28.31 ± 0.8	24.31 ± 0.9	28.2 ± 2.57
EBSD	RA	RA + 0.2Al5Ti1B	RA + 0.1Sc	RA + 0.3Sc	RA + 0.5Sc
Grain size (μm)	303.6 ± 50	203 ± 23	-	53.47 ± 7.1	45.9 ± 5.2
Grain refinement	–	33.1 %	–	82.4 %	84.9 %

Note: Grain refinement is calculated based on equation: Reduction(%) = $\frac{d_0 - d}{d_0} \times 100$.

rich. These needle-like particles were identified to be $Al_3(Sc,Ti)$ with selected area diffraction pattern (SAED) and HAADF plus STEM-EDS. More details in identification of $Al_3(Sc,Ti)$ can be found in our recent publication. The SAED patterns viewed from [100], [110], and [211] direction well identified the $Al_3(Sc,Ti)$ with LI_2 structure and well coherent with α-Al matrix. The HAADF and indexed SAED image was shown in Fig. 4l. The other elements such as Mg (Fig. 4e), Si (Fig. 4f), Cu (Fig. 4g), within the RA alloy were slightly segregated and formed fine SPPs at the boundary between eutectic cells and the Al matrix.

No α-Al twins have been reported under casting conditions, except under high-strain deformation [19,20]. In this study, the α-Al twins are observed for the first time and are primarily attributed to the constraint imposed by $Al_3(Sc,Ti)$, which is prone to twinning. The α-Al matrix and $Al_3(Sc,Ti)$ are highly coherent. Consequently, the twinning behaviour of $Al_3(Sc,Ti)$, as one of the eutectic phases, induces the formation of α-Al twins within these eutectic cells. These results also demonstrate that $Al_3(Sc,Ti)$ acts as the leading phase in the formation of these eutectic structures.

4. Discussion

4.1. Formation mechanism of eutectic $Al_3(Sc,Ti)$ + α-Al

Thermodynamic calculations using Pandat under the Scheil solidification model was displayed in Fig. 5. Fig. 5a indicates that the eutectic composition of the binary Al-Sc system is approximately 0.57 wt.% Sc. In addition, the solidification window for α-Al is extremely narrow, spanning only ~0.1 K. Fig. 5b shows the phase diagram of Al-0.5Sc-*x*Ti ternary alloys system. It shows that the phase diagram turns into peritectic, and only primary Al_3Ti can form when the concentration over 0.137 wt.%. However, in multi-component recycled Al alloys (RA-*x*Sc), the solidification behaviour of primary Al_3Sc changes significantly, as illustrated in Fig. 5c. In these alloys, equilibrium Al_3Sc formation requires a much higher Sc content (≥1.94 wt.%).

The calculated solidification paths for binary Al-1Sc and RA + 0.5Sc alloys are presented in Fig. 5e, while Fig. 5d shows the Scheil solidification curve for RA + 0.5Sc. The results indicate that Al_3Ti is the first phase to solidify in RA + 0.5Sc, rather than Al_3Sc. No Al_3Sc was expected to be solidified according to this calculation.

These calculations provide insight into the solidification sequence of multi-component recycled Al alloys with Sc additions, particularly the competitive formation of Al_3X (Sc/Ti) phases prior to α-Al solidification. However, it is important to note the limitations of the current thermodynamic database, which may not fully capture phase modifications or transitions, such as Ti incorporation into $Al_3(Sc,Ti)$, as reported in our recent work. This also highlights the broader limitations of thermodynamic modelling in complex multi-component alloy systems.

In multi-component recycled Al alloys containing Sc and Ti together with common impurity elements (Si, Cu, Zn, Fe, Mn, Mg, Cr), the formation behaviour of Al_3X phases becomes significantly more complex compared with binary Al-Sc or ternary Al-Sc-Ti systems. Unlike the binary case where Al_3Sc forms directly once the local Sc concentration exceeds its solubility limit, the presence of Ti and other alloying/impurity elements introduces strong thermodynamic competition during solidification. Ti preferentially forms Al_3Ti early in the solidification sequence, which alters the residual liquid composition and can effectively delay or suppress Al_3Sc formation. At the same time, mutual substitution between Sc and Ti within the $L1_2$ structure leads to the formation of $Al_3(Sc,Ti)$, further coupling their phase stability rather than allowing independent intermetallic formation. Additional solutes such as Fe, Si, and Cu continuously modify activity coefficients, partitioning behaviour, and the chemical potential of Al in the liquid, thereby shifting the driving force for Al_3X precipitation and narrowing the α-Al

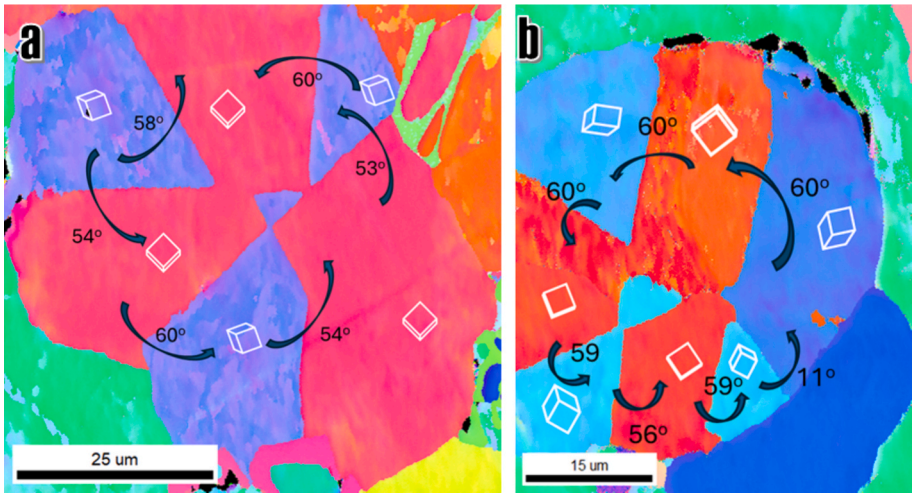

Fig. 2. EBSD-IPF images of eutectic cells showing the misorientation angles between adjacent grains. (a) Al crystals exhibiting a 54–60° misorientation between adjacent grains; (b) region showing a 56–60° misorientation.

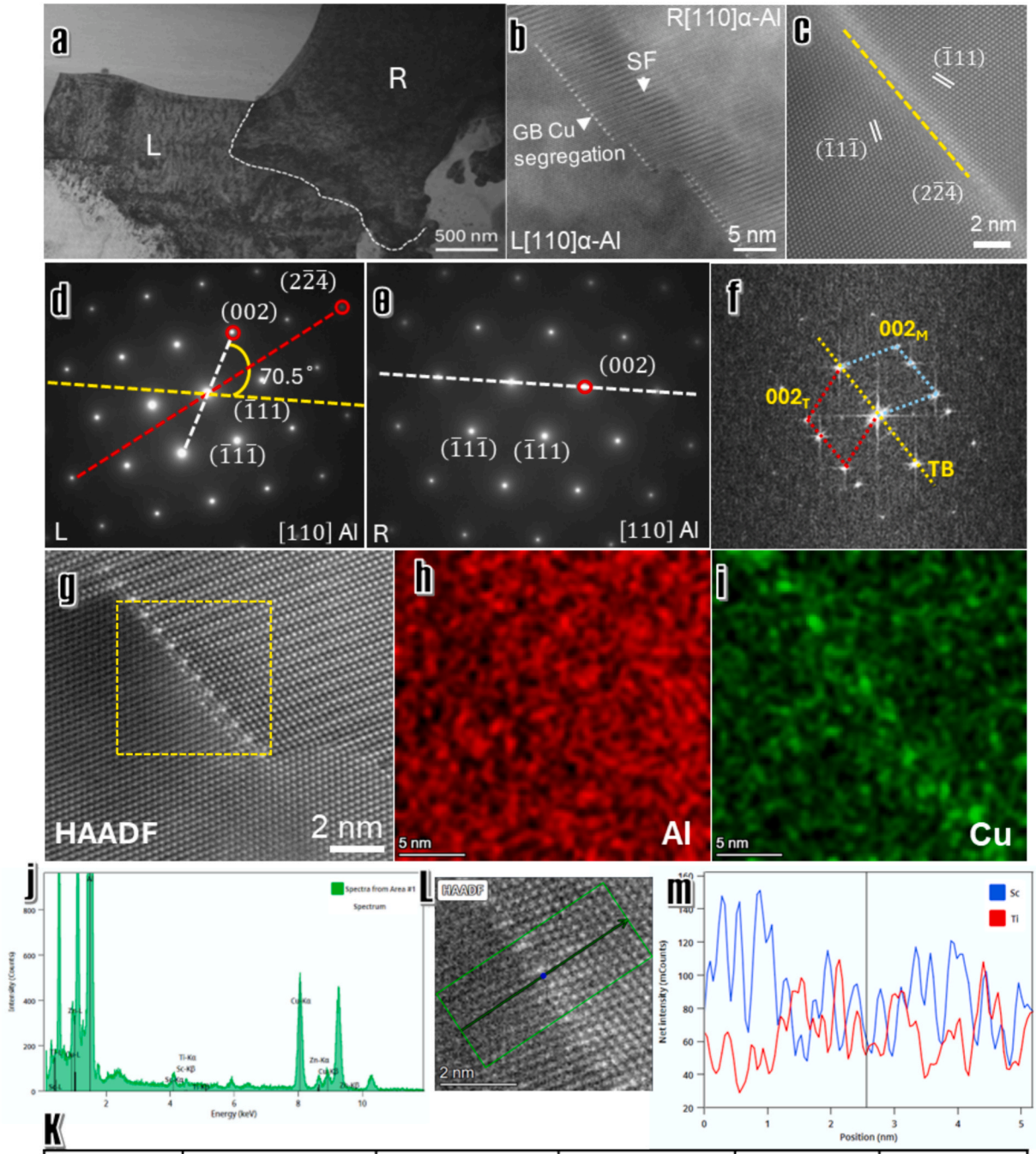

Element	Atomic Fraction (%)	Atomic Error (%)	Mass Fraction (%)	Mass Error (%)	Fit Error (%)
Al	97.36	0.31	94.10	0.69	0.41
Sc	0.16	0.02	0.26	0.03	1.45
Ti	0.03	0.01	0.05	0.01	10.98
Cu	2.22	0.31	5.05	0.69	0.60
Zn	0.23	0.03	0.54	0.07	1.11

Fig. 3. α-Al twins observed in eutectic cells of RA-0.3 wt.% Sc alloy. (a) Low-magnification bright-field TEM image highlighting a twin boundary (TB) with corresponding SAED patterns (d, e) showing {112} twin planes. (b and c) HAADF-STEM images detailing the twin boundary, including stacking faults and boundary-associated solute segregation; (f) FFT of image (c). (g–i) STEM-EDS maps of the twin boundary showing Cu segregation; (j) STEM-EDS spectrum acquired from the region highlighted by the yellow frame in (g), with the corresponding quantified composition presented in (k); (l) STEM-EDS line scan performed across the twin boundary; and (m) the corresponding intensity profiles of Sc and Ti.

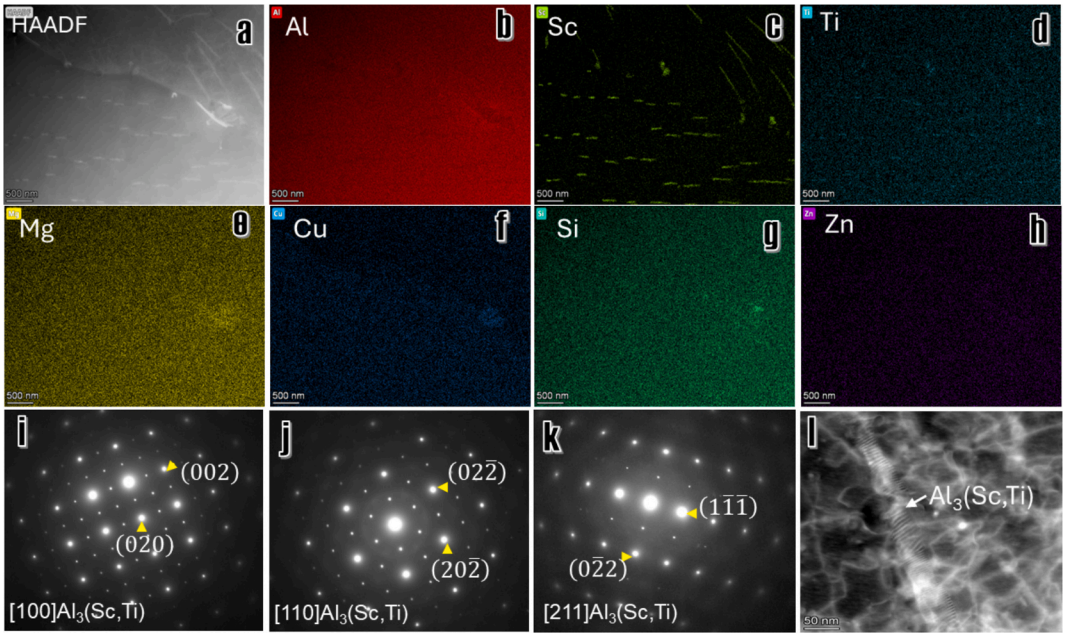

Fig. 4. Elemental mapping of a eutectic cell in RA-0.3 Sc alloy, showing needle-like $Al_3(Sc,Ti)$ precipitates and elemental segregation at the cell boundary. (a) HAADF image of the eutectic cell interface; corresponding STEM-EDS maps of (b) Al, (c) Sc, (d) Ti, (e) Mg, (f) Cu, (g) Si, and (h) Zn. Selected-area electron diffraction (SAED) patterns showing $Al_3(Sc,Ti)$ and α-Al along (i) [100], (j) [110], and (k) [211] zone axes. (l) HAADF image of an $Al_3(Sc,Ti)$ needle viewed along the [211] zone axis.

solidification window. Consequently, the Al_3X phase in these multi-component systems should be viewed not as a single stoichiometric endpoint but as a compositionally evolving intermetallic family governed by coupled thermodynamic interactions and non-equilibrium solidification pathways, which also explains the significantly higher Sc threshold required for equilibrium Al_3Sc formation in recycled alloy matrices.

According to phase diagram calculations, primary Al_3Sc is not expected to form, whereas some primary Al_3Ti may form during the solidification process. However, in the present study, no primary Al_3X intermetallic compounds were observed in either the RA alloy without Sc addition or in samples with Sc additions up to 0.5 wt.%. Although experimental observation of primary $Al_3(Sc,Ti)$ particles is challenging, particularly when their size is very small (<1-2 μm). These particles possess a crystal structure closely matching that of Al and exhibit a similar dissolution behaviour during sample preparation, making them difficult to detect using conventional etching, SEM, EBSD techniques. This issue will be discussed in detail in the future publication. Nevertheless, the samples across length scales ranging from micrometres to nanometres using SEM-EDS analysis have been carefully examined. No primary Al_3X particles were observed in all the samples of this study. The suppression of Al_3X formation may be attributed to nucleation difficulties and the metastable casting conditions, analogous to those observed for Fe-containing intermetallic compounds (Fe-IMCs) [25].

Therefore, microstructural refinement is dominated by the formation of eutectic cells, which nucleate and grow after the solidification of primary α-Al grains, preferentially along grain boundaries and secondary dendrite arms. These cells restrict α-Al grain growth, effectively subdividing large grains and producing significant grain refinement.

Optical images (Figs. 1c-3 and 1e-3) show that α-Al solidifies firstly in RA alloys cast at 3.5 K/s. The ($Al_3(Sc,Ti)$ + α-Al) eutectic solidifies immediately after α-Al but before other SPPs, causing the eutectic cells to grow along developing α-Al dendrites and distribute within dendritic arms. Compared to 0.5 wt.% Sc, 0.3 wt.% Sc is further from the eutectic composition, resulting in a lower volume fraction of eutectic cells.

As primary α-Al dendrites grow, solute elements, including Sc are rejected into the remaining melt, enriching local regions between dendrite arms. The solidification window for α-Al in Al-Sc is narrow (<1 K) (Fig. 5a), so when the composition and temperature undercooling reach the eutectic point, the ($Al_3(Sc,Ti)$ + α-Al) eutectic forms and propagates along the interdimeric regions.

4.2. *Grain Refinement mechanism by formation of ($Al_3(Sc,Ti)$ + α-Al) eutectic cells*

To fully understand the grain refinement induced by Sc addition in the absence of primary Al_3Sc formation, but with the presence of (Al_3Sc + Al) eutectic cells, the solute effect must be considered. Compared to the reference alloy (RA), the addition of Sc up to 0.5 wt.% results in significant grain refinement (Fig. 1). The solute effect associated with growth restriction can be evaluated using the growth restriction factor, Q [26] with equation of $Q = m_L(k-1)C_o$. Where, m_L and k are independent of solute content C_o and Q is then proportional to C_o.

Based on calculations for binary Al-Sc alloys, the Q values are 0.13 for 0.3 wt.% Sc and 0.22 for 0.5 wt.% Sc, which are significantly lower than those for Ti-containing alloys. For example, Q reaches 88.89 at 0.3 wt.% Ti and remains as high as 26.67 even at 0.09 wt.% Ti.

These results indicate that solute-based growth restriction from Sc is relatively weak. Instead, due to the very close formation temperatures of the eutectic cells and α-Al, the ($Al_3(Sc,Ti)$ + Al) eutectic forms early and develops into cells with sizes up to several tens of micrometres. These eutectic cells impose a strong physical restriction on the growth of α-Al dendrites, effectively truncating their development. Therefore, the observed grain refinement in this study represents a unique mechanism, where Sc addition promotes the formation of ($Al_3(Sc,Ti)$ + Al) eutectic cells that act as physical barriers, rather than relying primarily on conventional solute-driven growth restriction.

A schematic of the grain refinement mechanisms in RA alloys with different additions is shown in Fig. 6. Without any additions, α-Al nucleates on native sites and grows into large grains, with SPPs distributed within the dendritic arms. With a commercial Al-Ti-B grain refiner, α-Al grains nucleate on potent TiB_2 particles, forming a cellular morphology, while SPPs coarsen at the grain boundaries. In contrast, with 0.3–0.5 wt.% Sc, twinned eutectic cells of ($Al_3(Sc,Ti)$ + α-Al) form after primary

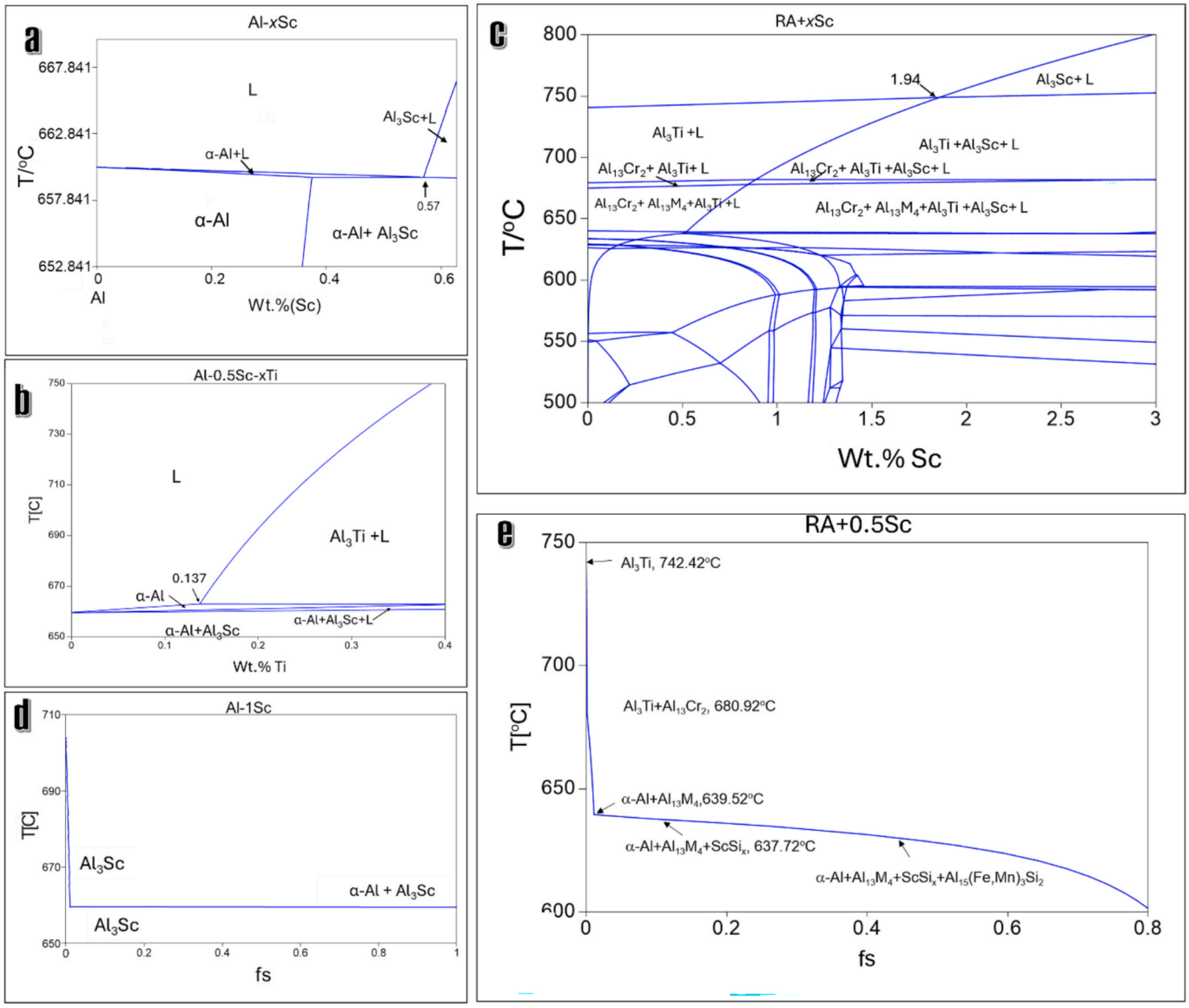

Fig. 5. Calculated phase diagrams using the Scheil model for (a) Al-*x*Sc binary alloy system; (b) Al-0.5Sc-xTi ternary alloy system; (c) RA-*x*Sc alloys; and solidification curves for (d) Al-1Sc and (e) RA-0.5Sc.

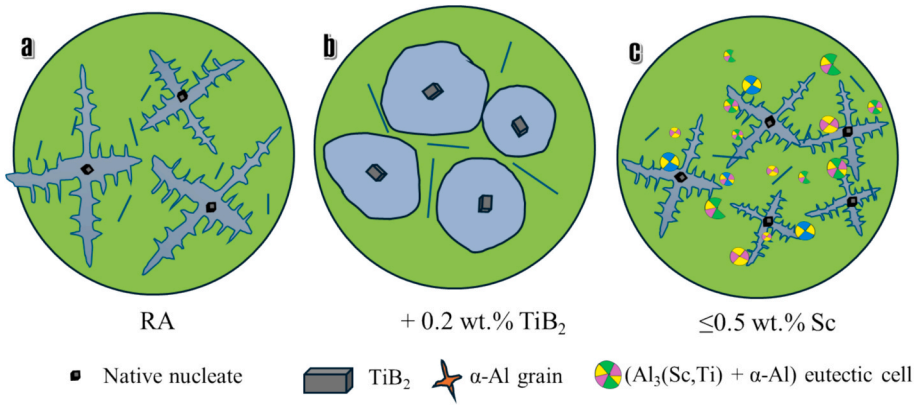

Fig. 6. Schematic illustration of grain refinement mechanisms in RA alloys: (a) without any addition, (b) with 0.2 wt.% Al-5Ti-1B, and (c) with 0.3–0.5 wt.% Sc.

α-Al solidification. These cells restrict the growth of α-Al dendrites, achieving significant grain refinement without disrupting secondary dendrite arm development. This approach simultaneously preserves fine SPPs within the dendritic arms and minimizes coarse SPP accumulation

at grain boundaries, offering the combined benefits of grain refinement and controlled SPP distribution (Fig. 6c).

4.3. Twinning mechanism of α-Al

In RA alloys with Sc additions, EBSD (Fig. 1d-1) and TEM analyses (Fig. 2) reveal α-Al twins within the (Al_3(Sc,Ti) + α-Al) eutectic cells. These twins exhibit characteristic {112} twin planes, confirmed by SAED and high-resolution HAADF-STEM imaging. Twinning in as-cast α-Al is unusual due to its high stacking fault energy (SFE), which typically suppresses twin formation during solidification. The crystallographic indexing has been re-examined, confirming that the twin plane is {112}, rather than the conventional {111} plane typically observed in FCC metals. This deviation is attributed to a different formation mechanism. In most previously reported cases, Al twins form under significant plastic deformation, where the {111} close-packed plane is favoured as the twinning plane to accommodate dislocation activity in an energetically efficient manner. In contrast, the Al twins reported in this work form under as-cast conditions, without external deformation or large applied strain. Instead, their formation is associated with coupled growth involving Al_3(Sc,Ti) intermetallic compounds. As a result, the twinning habit is governed by the intrinsic growth behaviour of the Al_3(Sc,Ti) phase rather than deformation-driven mechanisms. Further investigation is ongoing to fully elucidate this mechanism.

Under metastable casting conditions, the (Al_3(Sc,Ti) + α-Al) eutectic forms once the local composition and undercooling reach the eutectic point. Within the eutectic cells, Al_3(Sc,Ti) and α-Al grow in a coupled and coherent way (Fig. 4a). The Al_3(Sc,Ti) solidified at the high temperature exhibits a relatively high tolerance to impurity elements. To accommodate lattice strain induced by impurity segregation, twinning may occur during the growth of Al_3(Sc,Ti), consistent with previously reported twinned structures in Al_3Sc [27]. The twinning of Al_3(Sc,Ti) can subsequently induce corresponding twinning in the coupled α-Al phase due to their crystallographic relationship during eutectic growth. Furthermore, twinning within the eutectic does not originate from a discrete nucleation event; rather, it develops as a continuous crystallographic transition along the coupled solidification interface (Fig. 1d-2).

In addition, a recent paper demonstrated that the presence of Sc is expected to modify the stacking fault energy, which may facilitate twin formation during solidification [18,19], which also explain why the as-cast Al twin can be observed in this study. Additionally, the coupled eutectic growth front may impose local crystallographic constraints, favouring the development of specific twin relationships within the eutectic cells.

The lattice strain observed in α-Al, such as stacking default (Fig. 3b), can be attributed to impurities trapped during high-temperature solidification. The elemental segregation observed, i.e. Cu enrichment at twin boundaries (Fig. 3i), further supports this interpretation. In the present study, the twins are considered to form prior to significant dislocation activity. Under high-temperature solidification conditions and given the relatively impurity tolerance, solute elements in the α-Al matrix are not thermodynamically stable and tend to segregate. Twin boundaries, which possess higher interfacial energy than the surrounding matrix, act as preferential sites for solute segregation. This segregation can further stabilize the twin structures once formed. Moreover, under non-equilibrium solidification conditions, twinning can serve as an effective mechanism for accommodating lattice strain, especially when conventional dislocation motion is restricted.

This mechanism demonstrates that solute enrichment, spatial confinement by eutectic cells, and local undercooling collectively facilitate twin formation in high-SFE α-Al. The resulting twinning subdivides the microstructure and enhances overall grain refinement in RA alloys with Sc. Moreover, the impurity tolerance of the eutectic cells, represented as fine precipitates within and along their boundaries (Fig. 1d-2), further refines SPPs of as-cast microstructure and boundary structures, potentially enhancing the mechanical properties of RA alloys through Sc addition.

The growth twins observed in α-Al are formed within the (Al_3(Sc,Ti) + α-Al) eutectic cells during solidification. In this coupled growth process, the Al_3(Sc,Ti) phase acts as the leading phase and establishes a confined interfacial environment that governs the subsequent solidification of the surrounding α-Al. Although Al_3(Sc,Ti) does not directly impose a specific crystallographic twinning plane onto α-Al, the coherency between Al and Al_3(Sc,Ti) phase means that Al growth will be different based on the local conditions within the eutectic cells. As the solid/liquid interface advances, these conditions promote correlated atomic attachment and stacking sequence fluctuations in the adjacent α-Al, thereby enabling the formation of growth twins. This mechanism highlights that twin formation in α-Al observed during casting is primarily controlled in this case by eutectic-cell-mediated interfacial constraints and coupled solidification behaviour and is not related to the conventional twinning observed with deformation or recrystallisation in FCC metals that that requires dislocation mediation.

4.4. Advances and prospects of Scandium in Aluminium alloys

Heterogeneous nucleation is indeed a rapid and effective approach for grain refinement. Firstly, grain refinement is commonly employed to reduce casting defects such as hot tearing and can enhance mechanical performance through the Hall–Petch effect by increasing grain boundary density. However, several important aspects should be considered when reimaged on future sustainable Al alloys development. Nevertheless, grain refinement may also lead to the formation of relatively coarse second-phase particles, as larger intergranular regions can remain after refinement. In recycled Al alloys, this can be detrimental due to their limited impurity tolerance. In contrast, without conventional grain refinement, finer secondary dendrite arm spacing (SDAS) and more refined second-phase particles (SPPs) can often be achieved.

In this study, we report a novel phenomenon: with Sc addition below the eutectic composition (typically ~0.3 wt.%), both refined grain size and reduced SDAS can be simultaneously obtained. At the same time, refined SPPs and enhanced impurity tolerance are achieved, which we attribute to the increased boundary density introduced by twinned eutectic cells. This advantage is closely associated with the unique microstructural features identified in this work, as revealed by EBSD and polarized optical microscopy.

Although scandium (Sc) is more expensive than conventional grain refiners i.e. Al-5Ti-1B, our forthcoming publication demonstrates its superior recyclability in aluminium alloys over multiple recycling cycles. Unlike traditional grain refiners, which are typically effective only once which therefore request top-up and potentially introduce inclusions and impurities (i.e. Ti) during recycling loops [28], scandium remains effective throughout repeated reuse.

This makes Sc a more sustainable and long-term alloying element. Its benefits extend beyond improving the as-cast microstructure; it also enhances performance during subsequent processing steps, including thermomechanical processing and heat treatment, ultimately leading to improved mechanical properties [29,30]. A systematic and in-depth investigation is essential to fully understand the scientific role of scandium (Sc) in recycled aluminium alloys before effective technologies can be developed to minimise its usage while maximising its benefits.

5. Conclusions

In this study, a novel grain refinement mechanism in a recycled multi-component Al alloy was demonstrated via hypoeutectic Sc addition. Unlike conventional Al-Ti-B refinement, grain subdivision occurs through the formation of twinned (Al_3(Sc,Ti) + α-Al) eutectic cells, which nucleate after primary α-Al solidification and caused the spatial confinement of α-Al dendrites. EBSD and anodized optical analyses show that these eutectic cells, combined with twin formation, produce a highly refined microstructure, achieving up to 84.9 % effective grain

refinement at 0.5 wt.% Sc. The eutectic cells also preserve fine SPPs within dendritic arms while minimizing coarse SPP accumulation at grain boundaries, owing to their impurity tolerance and solute segregation. This dual effect, microstructural subdivision and SPP refinement, offers a promising strategy for enhancing the mechanical performance of recycled Al alloys. Overall, hypoeutectic Sc additions provide an efficient approach to simultaneously refine α-Al grains, stabilize secondary phases, and control microstructural features in complex, sustainable Al alloys.

CRediT authorship contribution statement

Zhongping Que: Writing – review & editing, Writing – original draft, Visualization, Validation, Supervision, Resources, Methodology, Investigation, Funding acquisition, Formal analysis, Data curation, Conceptualization. **Zhichao Niu:** Investigation. **Chamini L. Mendis:** Investigation. **Raluca Florentina Negrea:** . **Zhongyun Fan:** Investigation, Funding acquisition.

Funding

This work was financial supported by the EPSRC (UK) under grant number EP/N007638/1 (Future Liquid Metal Engineering Hub) and by Brunel University of London BRIEF award (11937131).

Declaration of competing interest

The authors declare that they have no known competing financial interests or personal relationships that could have appeared to influence the work reported in this paper.

Data availability

Data will be made available on request.

References

[1] S. Tian, Y. Di, M. Dai, W. Chen, Q. Zhang, Comprehensive assessment of energy conservation and CO_2 emission reduction in future aluminum supply chain, Appl. Energy. 305 (2022) 117796.
[2] Z. Yang, G. Fang, W. Sun, Embodied carbon emissions and their transfer pathways in global aluminum trade: the value chain perspective, Clean. Prod. 494 (2025) 145057.
[3] A. Sarkar, N. Razavi, G. Ringen, T. Welo, Assessing the fatigue behaviour of recycled Al-alloys: a critical review, Materialia 32 (2023) 101938.
[4] H. Nunes, O. Emadinia, R. Soares, M.F. Vieira, A. Reis, Adding value to secondary aluminum casting alloys: a review on trends and achievements, Materials 16 (3) (2023) 895.
[5] H.W. Doty, H.R. Ammar, A.M. Samuel, V. Songmene, F.H. Samuel, Effect of alloy composition, solidification rate, porosity level, grain refining and modification on the performance of aluminum-based alloys, J. Mater. Enger. Perform. 35 (2026) 5002–5031.
[6] M.A. Easton, M. Qian, A. Prasad, D.H. StJohn, Recent advances in grain refinement of light metals and alloys, Curr. Opin. Solid State Mater. Sci. 20 (2016) 13–24.
[7] Z. Liu, Review of grain refinement of cast metals through inoculation: theories and developments, Metal. Mater. Trans. A 48 (2017) 4755–4776.
[8] S. Liu, T. Zhao, J. Fu, Q. Zu, Development of inoculants for aluminum alloy: a review, Materials 16 (15) (2023) 5500.
[9] B.S. Murty, S.A. Kori, M. Chakraborty, Grain refinement of aluminium and its alloys by heterogeneous nucleation and alloying, Int. Mater. Rev. 47 (2002) 3–29.
[10] A.L. Geer, A.M. Bunn, A. Tronche, P.V. Evans, D.J. Bristow, Modelling of inoculation of metallic melts: application to grain refinement of aluminium by Al–Ti–B, Acta Mater. 48 (11) (2000) 2823–2835.
[11] Y. Wang, S. Wang, Z. Que, C. Fang, T. Hashimoto, X. Zhou, Q.M. Ramasse, Z. Fan, Manipulating nucleation potency of substrates by interfacial segregation: an overview, Metals 12 (2022) 1636.
[12] J. Røyset, N. Ryum, Scandium in aluminium alloys, Int. Mater. Rev. 50 (1) (2005) 19–44.
[13] J. Peng, W. Wang, J. Zeng, S. Yuan, L. Liu, J. Ji, S. Wu, Al3Sc phase uniform distribution and aluminium grains refinement in Al-2Sc alloy achieved by NdFeB permanent magnet stirring, J. Rare Earths. 43 (7) (2025) 1535–1547.
[14] D. Schimbäck, P. Mair, M. Bärtl, F. Palm, G. Leichtfried, S. Mayer, P.J. Uggowitzer, S. Pogatscher, Alloy design strategy for microstructural-tailored scandium-modified aluminium alloys for additive manufacturing, Scrip. Mater. 207 (2022) 114277.
[15] Q. He, T. Huang, L. Shuai, Y. Zhang, G. Wu, X. Huang, D.J. Jensen, In-situ investigation of the evolution of annealing twins in high purity aluminium, Scrip. Mater. 153 (2018) 68–72.
[16] E.B. Tadmor, N. Bernstein, A first-principles measure for the twinnability of FCC metals, J. Mech. Phys. Solids 52 (11) (2004) 2507–2519.
[17] B. Hammer, K.W. Jacobsen, V. Milman, M.C. Payne, Stacking fault energies in aluminium, J. Phys. Condens. Matter. 4 (50) (1992) 10453.
[18] L.H. Liu, J.H. Chen, T.W. Fan, Z.R. Liu, Y. Zhang, D.W. Yuan, The possibilities to lower the stacking fault energies of aluminum materials investigated by first-principles energy calculations, Comput. Mater. Sci. 108 (2015) 136–146.
[19] L.H. Liu, J.H. Chen, T.W. Fan, S.L. Shang, Q.Q. Shao, D.W. Yuan, Y. Dai, The stability of deformation twins in aluminum enhanced by alloying elements, J. Mater. Sci. Technol. 35 (11) (2019) 2625–2629.
[20] Q.F. Guan, Q.Y. Zhang, C. Dong, G.T. Zou, Deformation twining in single-crystal aluminum induced by high-current pulsed electron beam, J. Mater. Sci. 40 (18) (2005) 5049–5052.
[21] D. Bufford, Y. Liu, Y. Zhi, Z. Bi, Q.X. Jia, H. Wang, X. Zhang, Formation mechanisms of high-density growth twins in aluminum with high stacking-fault energy, Mater. Res. Lett. 1 (1) (2013) 51–60.
[22] B. Li, Y. Cao, K.T. Ramesh, E. Ma, A nucleation mechanism of deformation twins in pure aluminum, Acta Materialia 57 (15) (2009) 4500–4507.
[23] J. R. Davis. (Ed.). Aluminum and aluminum alloys. ASM International. (1993).
[24] Aluminium Association: Standard Test Procedure for Aluminium Alloy Grain Refiners: TP-1, Washington DC., (1987).
[25] Z. Que, Y. Wang, Z. Fan, T. Hashimoto, X.R. Zhou, Composition templating for heterogenous nucleation of intermetallic compounds, Sci. Rep. 14 (1) (2024) 8968.
[26] T.E. Quested, A.T. Dinsdale, A.L. Greer, Thermodynamic modelling of growth restriction effects in aluminium alloys, Acta Mater. 53 (5) (2005) 1323–1334.
[27] X.-Q. Wang, Y. Wang, Q. Jia, Z.-C. Ding, J.-J. He, S.-X. Hui, Novel twinned Al_3Sc dendrites in as-casted Al-Sc alloy, Rare Met. 42 (3) (2023) 838–843.
[28] Z. Niu, Z. Que, J.B. Patel, Z. Fan. Assessment and Improvement of Melt Quality of Recycled Secondary A357 Alloy by Application of the High Shear Melt Conditioning (HSMC) Technology. *Crystals,* 14(12) (20024) 1044.
[29] J.-Y. Zhang, Y.-H. Gao, C. Yang, P. Zhang, J. Kuang, G. Liu, J. Sun, Microalloying Al alloys with Sc: a review, Rare Metals 39 (2020) 636–650.
[30] C. Yang, P. Zhang, D. Shao, R.H. Wang, L.F. Cao, J.Y. Zhang, G. Liu, B.A. Chen, J. Sun, The influence of Sc solute partitioning on the microalloying effect and mechanical properties of Al-Cu alloys with minor Sc addition, Acta Mater. 119 (2016) 68–79.